Controlling independently the electric and thermal properties by shrinking the particle size down to nanosize in quasi-one-dimensional $Ca_3Co_2O_6$ and $Sr_6Co_5O_{15}$

Tsuyoshi Takami,[1,*] Munehisa Horibe,[1] Masayuki Itoh,[1] and Jinguang Cheng[2]
[1]*Department of Physics, Graduate School of Science, Nagoya University, Furo-cho, Chikusa-ku, Nagoya 464-8602, Japan*
[2]*Texas Materials Institute, University of Texas at Austin, 1 University Station C2201, Austin, Texas 78712, USA*
(Received 23 February 2010; revised manuscript received 3 July 2010; published 13 August 2010)

We report on the preparation of conventional and nanosized crystals of the quasi-one-dimensional compounds, $Ca_3Co_2O_6$ and $Sr_6Co_5O_{15}$, which are potential candidates for thermoelectric materials at higher temperatures; phonon scattering in nanosized crystals reduces the thermal conductivity. Simultaneous modification of the particle size and the oxygen content by milling processes is found to be critical not only for reducing the thermal conductivity, but also for improving an electrical conductivity, especially in the vicinity of compositions fulfilling the condition of a band insulator where one can control the sign of the thermoelectric power.

DOI: 10.1103/PhysRevB.82.085110 PACS number(s): 72.15.Jf, 72.20.Pa, 65.80.−g

I. INTRODUCTION

In thermoelectric materials, the application of a temperature gradient generates efficiently a voltage, and vice versa. The efficiency of thermoelectric energy converters is determined by the dimensionless figure of merit, $ZT=S^2T/\rho\kappa$, where S, T, ρ, and κ are the thermoelectric power, absolute temperature, electrical resistivity, and thermal conductivity, respectively. In order to achieve high thermoelectric performance, a low κ is required in addition to the coexistence of a large S and a low ρ. However, fulfilling this condition is usually not compatible because the thermoelectric factors, i.e., S, ρ, and κ, change monotonically with the carrier concentration, n.[1] In the early 1990s, an enhancement in ZT with nanostructures was proposed by Hicks and Dresselhaus.[2] For nanocomposites, when the grain size is smaller than the mean-free path of a phonon, additional phonon scattering at grain boundaries would occur and κ is thereby reduced. The idea based on this concept has been widely accepted, but most experimental efforts failed since the smaller grain also increases ρ with almost no alternation in S, resulting in a decrease in the power factor, S^2/ρ. Recently, a noticeable enhancement in ZT has been achieved only for conventional thermoelectric materials such as AgPbSbTe,[3] p-type BiSbTe,[4,5] and SiGe.[6–8] In contrast to these degenerate semiconductors, the discovery of a large S and a low ρ in $NaCo_2O_4$ opened exploration of oxide thermoelectric materials.[9] In general, they offer a number of potential advantages for applications; for example, stability in air, resistance to heat, availability at high T. Layered cobalt oxides such as Na_xCoO_2 and $[Ca_2CoO_3]_{0.62}CoO_2$, however, decompose at $\approx$1100 K.

The quasi-one-dimensional (Q1D) compound $Ca_3Co_2O_6$ is chemically stable up to at least 1300 K.[10] Mikami *et al.*[11] suggested that ZT of a $Ca_3Co_2O_6$ single crystal should reach 0.44 at 1300 K by extrapolating their data to higher T's. This compound is the first member ($n=1$) of the homologous series $A_{n+2}Co_{n+1}O_{3n+3}$ (A: alkaline-earth metal). Its unit cell includes a 1D CoO_3 chain structure between which A is located.[12,13] The CoO_3 chain forming a triangular lattice in the ab plane consists of one CoO_6 trigonal prism and n CoO_6 octahedra, which are face sharing and connected one dimensionally. Motivated by a low dimensionality and a geometric frustration, extensive investigations on the magnetic properties have been conducted.[14–19] Also systematic studies varying n from 1 to 5 have revealed that the $n=2$ compound, $Sr_4Co_3O_9$, exhibits the largest power factor among polycrystalline samples.[20] In addition to the thermoelectric properties of the $Ca_3Co_2O_6$ single crystal, those of the $Sr_6Co_5O_{14.3}$ single crystal have also been reported; this compound is an oxygen-nonstoichiometric phase of $Sr_6Co_5O_{15}$ ($A=Sr, n=4$), and its power factor at 900 K is comparable to that of a single crystal of $Ca_3Co_2O_6$.[21]

While most of the studies on thermoelectric oxides have been devoted to bulk single crystals and polycrystalline samples, to our knowledge not much work has been done on a nanocrystalline form except for thin films. As is well known, electricity is carried by electrons in solids, whereas heat is done by lattice vibrations, electrons, and other excitations. In particular, the phonon contribution to κ is quite large compared to the electron contribution for the present Q1D compounds, which means that the control of the phonon scattering is naturally critical to reduce κ. And also, ZT can be expressed only by S via the Wiedemann-Franz law ideally assuming no contribution from the phonon. The general criterion for applications, i.e., $ZT\geq 1$, can then be rewritten as $S\geq 160\ \mu V/K$. Therefore, the present study is motivated by the desire to find a route of lowering κ while maintaining or improving an electrical conductivity in oxide thermoelectric materials.

II. EXPERIMENTAL

The polycrystalline $Ca_3Co_2O_6$ and $Sr_6Co_5O_{15}$ samples were synthesized by solid-state reaction. A stoichimetric mixture of $CaCO_3$, $SrCO_3$, and Co_3O_4 was carefully well-ground and calcined at 850 °C for 24 h in air; then, the obtained powders were pressed into pellets and sintered several times at 880–900 °C for 24 h with slow cooling down to room temperature. For the preparation of nanosized particles, single-phase conventional powders were milled for 100 h in a ball mill at a speed of 400 rpm in the medium of ethanol using BALLMILL ANZ-51S of NITTO KAGAKU CO., LTD. After that, the milled powders were pelletized

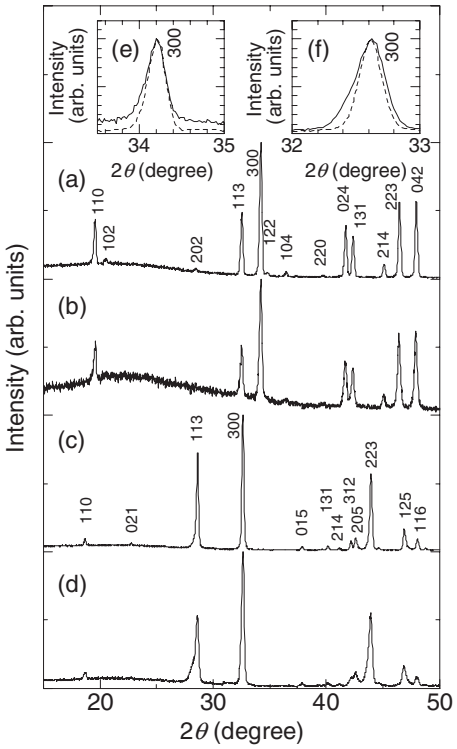

FIG. 1. X-ray powder diffraction patterns of (a) conventional $Ca_3Co_2O_6$ powders, (b) nanosized $Ca_3Co_2O_{6-\delta}$ powders, (c) conventional $Sr_6Co_5O_{15}$ powders, and (d) nanosized $Sr_6Co_5O_{15-\delta}$ powders. The insets show XRD patterns around the main peak of the (300) reflection for the samples with (e) $n=1$ and (f) $n=4$ in an expanded scale. The dashed and solid curves denote XRD patterns of conventional and nanosized powders, respectively.

again at the same pressure used for the bulk containing as-sintered powders. Finally, the pellets were sintered just during the heating and cooling processes in order to prevent the powders from promoting grain growth. X-ray diffraction (XRD) measurements were conducted with Cu $K\alpha$ radiation in a Rigaku diffractometer. The morphology and surface features of the obtained crystals were investigated by scanning electron microscopy (SEM) with an FE-SEM: JSM-6700F. Magnetization measurements were performed with a Quantum Design's superconducting quantum interference device magnetometer between 2 and 300 K. Electrical resistivity and thermoelectric power were measured with home-built equipment by a four-probe method. A steady-state method was used to measure the thermal conductivity. An apparent density of the pellets containing conventional powders was 85–90% of the theoretical density and decreased by 5% with decreasing particle size. The oxygen contents in all the samples studied were chemically determined by iodometric titration. As-sintered samples showed oxygen stoichiometry, whereas the oxygen contents in the $n=1$ and 4 samples containing nanoparticles were 5.95 and 14.8, respectively.

III. RESULTS

Figures 1(a) and 1(c) show the XRD patterns of as-sintered powders of $Ca_3Co_2O_6$ and $Sr_6Co_5O_{15}$, respectively.

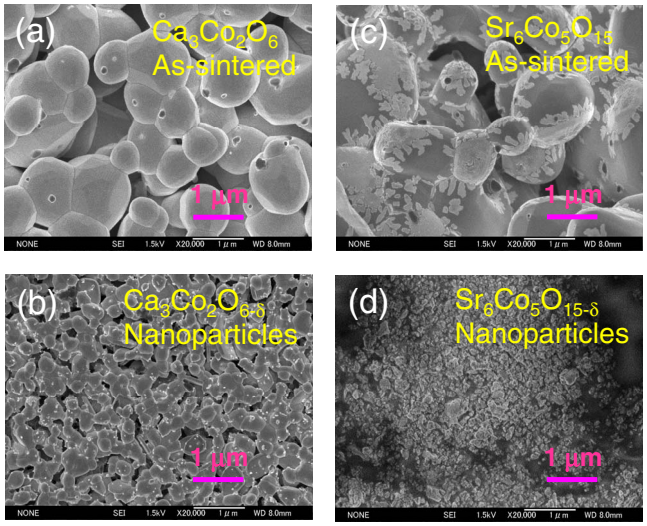

FIG. 2. (Color online) SEM photographs of (a) as-sintered $Ca_3Co_2O_6$, (b) $Ca_3Co_2O_{6-\delta}$ containing nanoparticles, (c) as-sintered $Sr_6Co_5O_{15}$, and (d) $Sr_6Co_5O_{15-\delta}$ containing nanoparticles. Note here that all the images are displayed on the same scale.

No impurity peaks were observed and all the peaks can be indexed by a rhombohedral structure, indicative of a single phase. The obtained lattice parameters are in fair agreement with the literature,[22,23] which also supports the oxygen stoichiometry in the present samples. In the case of milled powders, XRD peaks tended to be broader [see Figs. 1(b) and 1(d)]. For example, the full width at half maximum (FWHM) of the main peak of the (300) reflection for both compounds was clearly increased by the milling process [see Figs. 1(e) and 1(f)]. We roughly estimated the particle size of the samples by Scherrer's equation and the FWHM of the XRD spectra.[24] The particle size was found to decrease with milling; that is, it was estimated to be 205 and 59 nm for conventional and nanosized powders of $Ca_3Co_2O_6$, respectively. Similarly, the particle size of $Sr_6Co_5O_{15}$ was decreased from 409 to 102 nm by milling. These results imply a significant decrease in the particle size of both materials by milling. In order to obtain further information on the particle size, we have employed SEM measurements; SEM images for the present samples are shown in Fig. 2. It should be noted here that all the four figures are displayed on the same scale. As can be seen from Figs. 2(a) and 2(c), the particle sizes of the conventional powders of $Ca_3Co_2O_6$ and $Sr_6Co_5O_{15}$ are almost the same. After the powders were milled, the particle size was smaller for both samples, and the particles with a typical diameter of a few hundred nanometers attain nanometer dimensions with significant agglomeration.

Figure 3(a) shows the T dependence of ρ for $Ca_3Co_2O_6$. ρ of the nanosized sample is expected to increase because of a higher scattering of charge carriers due to the small grains. Surprisingly, ρ of the $Ca_3Co_2O_6$ pellets containing nanoparticles exhibited an opposite trend; namely, ρ is reduced. On the other hand, the absolute value of S also decreased with the particle size [see Fig. 3(b)]. Figure 3(c) shows the κ as a function of T for $Ca_3Co_2O_6$, in which κ of the conventional bulk is in fair agreement with an earlier report.[25] The bulk electron thermal conductivity (κ_e) of the conventional

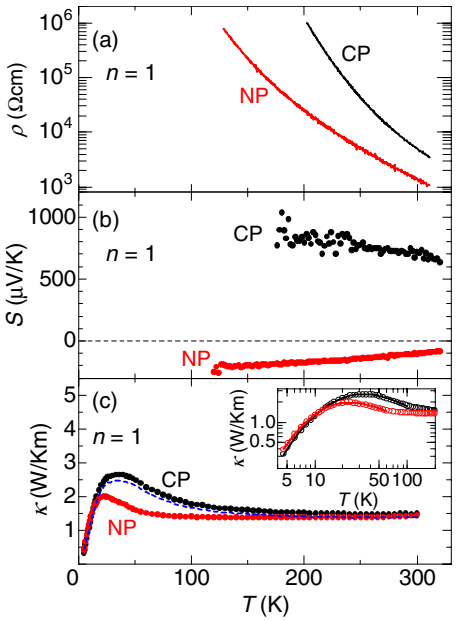

FIG. 3. (Color online) T dependences of (a) the electrical resistivity, (b) the thermoelectric power, and (c) the thermal conductivity for the $n=1$ compounds. The zero base line expressed by the dashed line in (b) is described to emphasize the negative value of the thermoelectric power observed for the sample containing nanoparticles. CP (black) and NP (red) represent the data of the conventional bulk and those of the bulk containing nanoparticles, respectively. The dashed curve denotes the κ excluded the porosity contribution. Lines in the inset of (c) are the fitting results with the Debye formula for phonon thermal conductivity.

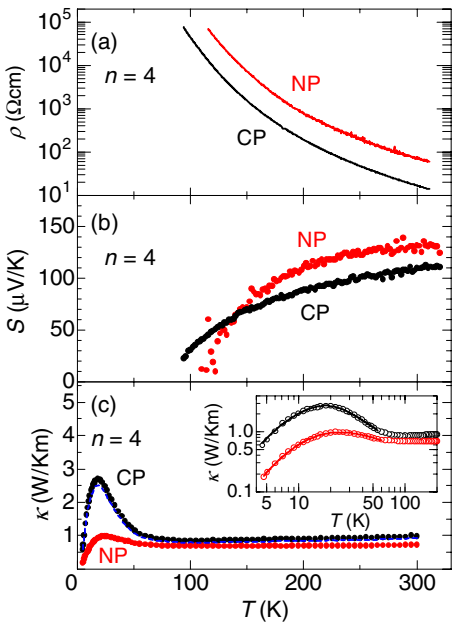

FIG. 4. (Color online) T dependences of (a) the electrical resistivity, (b) the thermoelectric power, and (c) the thermal conductivity for the $n=4$ compounds. CP (black) and NP (red) represent the bulk data of the conventional sample and those of the nanoparticles, respectively. The dashed curve denotes the κ excluded the porosity contribution. Lines in the inset of (c) are the fitting results with the Debye formula for phonon thermal conductivity.

and nanosized particles were estimated to be 1.48×10^{-7} W/K m and 5.34×10^{-7} W/K m at 300 K, respectively, by applying the Wiedemann-Franz law. In the T range measured, these values are negligible compared to the total κ. As mentioned above, κ_e is expected to increase with decreasing particle size by simply applying the Wiedemann-Franz law, resulting in an increase in κ assuming a constant phonon thermal conductivity (κ_{ph}) with no dependence on the particle size. κ of the nanosized sample, however, showed a distinct reduction compared to that of the as-sintered sample. In the case of $Sr_6Co_5O_{15}$, both ρ and S tended to increase, whereas κ was suppressed to below the quite low value of 1 W/K m by modifying the particle size, as we expected (see Fig. 4). Since the bulk κ_e of the conventional and nanosized particles was negligible, the reduction in κ cannot be explained by κ_e and thereby is also caused by the increased phonon scattering.

IV. DISCUSSION

First of all, we have compared κ of these ceramic samples with that of a single-crystal sample of $Ca_3Co_2O_6$. The overall κ at low T's is dramatically suppressed by about 2 orders in the ceramic samples.[26] We have estimated the porosity contribution to κ from the relation $\kappa/\kappa_0=1-(4/3)\phi$, where κ_0 is the corrected thermal conductivity for fully dense materials and ϕ is the fractional porosity.[27] The reduction in κ by shrinking the particle size down to nanosize is calculated to be $\approx7\%$ [see Figs. 3(c) and 4(c)], which means that the difference in κ between each other with the same n does not simply come from the bulk density. We have applied the Debye model to analyze the T dependence of κ at low T's. κ_{ph} is described with the Debye model as follows:[28]

$$\kappa_{ph}=\left(\frac{k_B}{2\pi^2 v}\right)\left(\frac{k_B}{\hbar}\right)^3 T^3\int_0^{\Theta_D/T}\frac{x^4e^x}{(e^x-1)^2}\tau dx, \qquad (1)$$

where k_B is the Boltzmann constant, $\hbar$ is the Planck's constant deviated by 2π, x is the normalized frequency $\hbar\omega/k_BT$, v is the speed of sound, and Θ_D is the Debye temperature of the present samples. Here, the relaxation time of a phonon can be expressed as

$$\tau^{-1}=v/L+A\omega^4+B\omega^3T\exp(-\Theta_D/bT). \qquad (2)$$

The first, second, and third terms are attributed to boundary scattering at the sample's boundary, phonon scattering by defects, and phonon-phonon scattering due to the umklapp (U) processes, respectively. All parameters from the single-crystal sample were used as the initial input for our fitting. For example, we tested the reliability by using Θ_D as a fitting parameter, but it changed little. Although it may be less reliable to apply the Debye model in the case of ceramic samples, the fitting still shows a dramatic difference in terms of the heat transfer by lattice vibrations [see the insets of Figs. 3(c) and 4(c)]. As expected, the grain dimension in the ceramic samples experienced by the phonon scattering is reduced by 3–4 orders relative to that of the single-crystal

TABLE I. Parameters of the fitting of $\kappa(T)$ to Eq. (1). Here, CP and NP represent conventional powders and nanopowders, respectively.

	$n=1$ (CP)	$n=1$ (NP)	$n=4$ (CP)	$n=4$ (NP)
Θ_D (K)	390	390	350	350
A (10^{-41} s^3)	1.59	2.00	1.71	3.99
B (10^{-30} K^{-1} s^2)	3.99	6.82	27.2	14.9
b	7.28	14.28	6.12	10.48
L (10^{-7} m)	9.07	12.3	23.4	52.2

samples. Moreover, the parameter A also increases in the ceramic samples, which indicates more defects such as surface states and oxygen vacancies in ceramic samples, Table I.

It is worth mentioning here that a large negative S, e.g., -195 μV/K at 150 K, is realized for $Ca_3Co_2O_6$ despite the difficulty in making the cobalt oxides n type. Thermodynamically, S is an entropy per carrier, and thus that of strongly correlated systems is known to depend on the density of charge carriers and on the spin state of the transition-metal ions.[29] In particular, in the vicinity of the composition for single-valent cobalt, the sign of S strongly depends on n, i.e., when the valence of cobalt ions is trivalent, S is divergent in the high-T limit; varying to the Co(III)/Co(IV) side brings about a positive value of S while varying to the Co(III)/Co(II) side makes S negative, as is shown in Fig. 5(a). For example, the ground state for $LaCoO_3$ is a nonmagnetic insulator with a low-spin (LS) state of Co(III).[34] Increasing the oxygen content changes S to a large positive S and reducing the oxygen content to a large negative S.[31] However, κ of $LaCoO_3$ is still high, e.g., $\approx$10 W/K m at 30 K.[31] And also, the absolute value of S for $LaCoO_3$ decreases rapidly above 500 K due to an insulator-metal transition and/or a spin-state transition of the Co(III).[35] Another way to realize a negative value of S for cobalt oxides is to change the valence to nearly all Co(IV), but unfortunately, access to all Co(IV) in oxides is frustrated by loss of oxygen. Other than cobalt oxides, the power factor of $La_{1-x}Sr_xTiO_3$ is comparable to that of a conventional thermoelectric material Bi_2Te_3, in which a large negative S together with a metallic conductivity is achieved, as is shown in Figs. 5(a) and 5(b). However, the ZT value is much less than unity in spite of the large power factor value because κ is an order of magnitude larger compared to that of Bi_2Te_3.

In the present case, Co ions in the prismatic and octahedral sites of as-sintered $Ca_3Co_2O_6$ have been reported to be in the high-spin (HS) state of Co(III) and the LS state of Co(III), respectively.[16,36] A negative S can be accounted for by an oxygen vacancy δ, i.e., electron doping, originating from the ball-milling processes, which is consistent with the results of iodometric titration. In addition to the decrease in ρ, the particle size variation in the effective magnetic moment (M_{eff}) derived from the magnetic susceptibility versus T curve also supports this scenario. Namely, M_{eff} decreased from 3.5 to 3.3μ_B with the particle size due to the HS state of Co(II) induced in the HS state matrix of Co(III), the former of which has a smaller spin quantum number. Although we measured the magnetic field variation in the magnetization

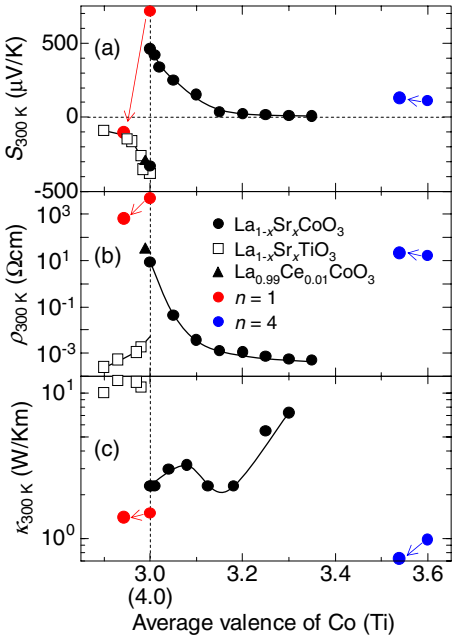

FIG. 5. (Color online) (a) Thermoelectric power, (b) electrical resistivity, and (c) thermal conductivity at room temperature as a function of the average valence of cobalt. The data for $La_{1-x}Sr_xCoO_3$ (Refs. 30 and 31), $La_{0.99}Ce_{0.01}CoO_3$ (Ref. 32), and $La_{1-x}Sr_xTiO_3$ (Ref. 33) are also plotted for comparison. In the case of $La_{1-x}Sr_xTiO_3$, the transverse axis is actually inadequate. The dashed lines to the longitudinal and transverse directions are described to emphasize the composition of a band insulator and the negative value of the thermoelectric power observed for $Ca_3Co_2O_{6-\delta}$, $La_{1-x}Sr_xTiO_3$, and $LaCoO_{3-\delta}$, respectively. The solid curves are guides to the eyes. It is noteworthy that the data of κ is plotted in logarithmic scale to stress a reduction in κ by shrinking the particle size down to nanosize.

(M) in order to directly extract the Co(II) concentration with the HS state, M of the sample containing the nanoparticles did not tend to saturate in the whole T range between 2 and 300 K even at 70 kOe. For $Ca_3Co_2O_6$ prepared by the sol-gel cum combustion method, the value of S with a positive sign is small and S increases with T.[37] Normally, the lattice constants increase with changing the average valence of Co ions from Co(IV) to Co(III). The smaller lattice constants, i.e., $a=9.04$ Å and $c=10.35$ Å, of this compound compared to those, i.e., $a=9.08$ Å and $c=10.38$ Å, of the oxygen stoichiometric sample indicates an excess oxygen content brings about this T variation in S. A sign change in S observed for the Ti(IV) doped compound, $Ca_3Co_{1.9}Ti_{0.1}O_6$, has also been interpreted by the same mechanism, but its ρ increases compared to $Ca_3Co_2O_6$ probably due to the modification of the cobalt valency and to the dilution of the Co network.[38] In accordance with this interpretation, the Zn(II) doped material, $Ca_3Co_{1.9}Zn_{0.1}O_6$, exhibits a positive value of S.[39] For $Sr_6Co_5O_{15}$, the particle size effect on S and ρ are qualitatively explained by the oxygen deficiency by milling. We emphasize here again that the significant difference observed in S and ρ for $Ca_3Co_2O_6$ and $Sr_6Co_5O_{15}$ is attributable to the initial average valence of Co ions.

In general, ρ increases for a mixed Co(III)/Co(II) valency due to a spin blockade phenomena.[40] As already discussed by

using the magnetization data, the band filling concerns only the Co with the HS state in the trigonal prism. Also, the local spin-density approximation+Hubbard U band-structure calculations support this scenario.[41] The spin blockade effect is not responsible for the electron transport in $Ca_3Co_2O_{6-\delta}$.

The main advantage of the nanocrystal approach for the present compounds is that one can reduce κ due to the increased phonon scattering even in oxide thermoelectric materials. Quite recently, although a reduction in κ for self-assembled nanostructured oxides, $Zn(Mn,Ga)O_4$, by the nanostructural effect was reported, ρ of the compounds is too high to measure.[42] Our experimental findings derived from the data of the $n=1$ system strongly suggest that milling processes for oxides have a positive effect on both the electrical and thermal conductivity, which is attributed to the change in the particle size and n as displayed in Fig. 5. Furthermore, our data on the $n=1$ system provides the first observation, as far as we know, of a lowering of κ while maintaining or improving the electrical conductivity in an oxide thermoelectric material. A signature guideline to improve thermoelectric performance of oxides can be proposed; it is to shrink the particle size down to nanosize at the single-valent composition in oxides thermoelectric materials in conjunction with suitable nanostructuring.

V. CONCLUSIONS

In conclusion, this work reveals several important experimental findings that are critical for improving the thermoelectric performance of oxide thermoelectric materials. We successfully prepared samples containing conventional and nanosized powders, which made it possible to address the effect of the particle size on the transport properties. Our study indicates (i) shrinking the particle size down to nanosize is also effective to reduce the thermal conductivity of thermoelectric oxides as expected, (ii) the simultaneous modification of the particle size and the oxygen content is useful not only for reducing the thermal conductivity, but also for maintaining or improving an electrical conductivity, especially in a band insulator or a Mott insulator, and (iii) a large negative thermoelectric power is realized in $Ca_3Co_2O_{6-\delta}$.

ACKNOWLEDGMENTS

This work was partly performed in Nanotechnology Support Project in Central Japan (Institute for Molecular Science), financially supported by Nanotechnology Network of the Ministry of Education, Culture, Sports, Science and Technology (MEXT), Japan. T.T. gratefully acknowledges the support by the Grant-in-Aid for Scientific Research (Grant No. 21740251) from the Japan Society for the Promotion of Science, the support by the Sasakawa Scientific Research Grant from the Japan Science Society, and the support by the Research Foundation for the Electrotechnology of Chubu.

*takami.tsuyoshi@g.mbox.nagoya-u.ac.jp

[1] G. Mahan, B. Sales, and J. Sharp, Phys. Today **50**(3), 42 (1997).
[2] L. D. Hicks and M. S. Dresselhause, Phys. Rev. B **47**, 12727 (1993).
[3] F. K. Hsu, S. Loo, F. Guo, W. Chen, J. S. Dyck, C. Uher, T. Hogan, E. K. Polychroniadis, and M. G. Kanatzidis, Science **303**, 818 (2004).
[4] B. Poudel, Q. Hao, Y. Ma, Y. C. Lan, A. Minnich, B. Yu, X. Yan, D. Z. Wang, A. Muto, D. Vashaee, X. Chen, J. M. Liu, M. S. Dresselhaus, G. Chen, and Z. F. Ren, Science **320**, 634 (2008).
[5] Y. Ma, Q. Hao, B. Poudel, Y. C. Lan, B. Yu, D. Z. Wang, G. Chen, and Z. F. Ren, Nano Lett. **8**, 2580 (2008).
[6] X. W. Wang, H. Lee, Y. C. Lan, G. H. Zhu, G. Joshi, D. Z. Wang, J. Yang, A. J. Muto, M. Y. Tang, J. Klatsky, S. Song, M. S. Dresselhuas, G. Chen, and Z. F. Ren, Appl. Phys. Lett. **93**, 193121 (2008).
[7] G. Joshi, H. Lee, Y. C. Lan, X. W. Wang, G. H. Zhu, D. Z. Wang, A. J. Muto, M. Y. Tang, M. S. Dresselhuas, G. Chen, and Z. F. Ren, Nano Lett. **8**, 4670 (2008).
[8] G. H. Zhu, H. Lee, Y. C. Lan, X. W. Wang, G. Joshi, D. Z. Wang, J. Yang, D. Vashaee, H. Guilbert, A. Pillitteri, M. S. Dresselhaus, G. Chen, and Z. F. Ren, Phys. Rev. Lett. **102**, 196803 (2009).
[9] I. Terasaki, Y. Sasago, and K. Uchinokura, Phys. Rev. B **56**, R12685 (1997).
[10] C. Brisi and P. Rolando, Ann. Chim. (Rome) **58**, 676 (1968).
[11] M. Mikami, R. Funahashi, M. Yoshimura, Y. Mori, and T. Sasaki, J. Appl. Phys. **94**, 6579 (2003).
[12] K. Boulahya, M. Parras, and J. M. González-Calbet, J. Solid State Chem. **142**, 419 (1999).
[13] K. Boulahya, M. Parras, and J. M. González-Calbet, J. Solid State Chem. **145**, 116 (1999).
[14] T. Takami, H. Nozaki, J. Sugiyama, and H. Ikuta, J. Magn. Magn. Mater. **310**, e438 (2007).
[15] V. Hardy, S. Lambert, M. R. Lees, and D. McK. Paul, Phys. Rev. B **68**, 014424 (2003).
[16] J. Sugiyama, H. Nozaki, J. H. Brewer, E. J. Ansaldo, T. Takami, H. Ikuta, and U. Mizutani, Phys. Rev. B **72**, 064418 (2005).
[17] J. Sugiyama, H. Nozaki, Y. Ikedo, K. Mukai, D. Andreica, A. Amato, J. H. Brewer, E. J. Ansaldo, G. D. Morris, T. Takami, and H. Ikuta, Phys. Rev. Lett. **96**, 197206 (2006).
[18] S. Aasland, H. Fjellvåg, and B. Hauback, Solid State Commun. **101**, 187 (1997).
[19] H. Kageyama, K. Yoshimura, K. Kosuge, H. Mitamura, and T. Goto, J. Phys. Soc. Jpn. **66**, 1607 (1997).
[20] T. Takami, H. Ikuta, and U. Mizutani, Jpn. J. Appl. Phys., Part 1 **43**, 8208 (2004).
[21] K. Iwasaki, T. Murase, T. Itoh, M. Yoshino, T. Matsui, T. Nagasaki, and Y. Arita, Jpn. J. Appl. Phys., Part 1 **46**, 256 (2007).
[22] H. Fjellvåg, E. Gulbrandsen, S. Aasland, A. Olsen, and B. C. Hauback, J. Solid State Chem. **124**, 190 (1996).
[23] K. Iwasaki, T. Ito, T. Matsui, T. Nagasaki, S. Ohta, and K. Koumoto, Mater. Res. Bull. **41**, 732 (2006).
[24] P. Scherrer, Nachr. Ges. Wiss. Goettingen, Math.-Phys. Kl. **26**, 98 (1918).

[25] A. Maignan, S. Hébert, C. Martin, and D. Flahaut, Mater. Sci. Eng., B **104**, 121 (2003).
[26] J.-G. Cheng, J.-S. Zhou, and J. B. Goodenough, Phys. Rev. B **79**, 184414 (2009).
[27] K. W. Schlichting, N. P. Padture, and P. G. Klemens, J. Mater. Sci. **36**, 3003 (2001).
[28] R. Berman, *Thermal Conduction in Solids* (Clarendon, Oxford, 1976).
[29] W. Koshibae, K. Tsutsui, and S. Maekawa, Phys. Rev. B **62**, 6869 (2000).
[30] T. Takami, H. Ikuta, and U. Mizutani, Trans. Mater. Res. Soc. Jpn. **29**, 2777 (2004).
[31] K. Berggold, M. Kriener, C. Zobel, A. Reichl, M. Reuther, R. Müller, A. Freimuth, and T. Lorenz, Phys. Rev. B **72**, 155116 (2005).
[32] A. Maignan, D. Flahaut, and S. Hébert, Eur. Phys. J. B **39**, 145 (2004).
[33] T. Okuda, K. Nakanishi, S. Miyasaka, and Y. Tokura, Phys. Rev. B **63**, 113104 (2001).
[34] J. B. Goodenough, J. Phys. Chem. Solids **6**, 287 (1958).
[35] J.-Q. Yan, J.-S. Zhou, and J. B. Goodenough, Phys. Rev. B **69**, 134409 (2004).
[36] K. Takubo, T. Mizokawa, S. Hirata, J.-Y. Son, A. Fujimori, D. Topwal, D. D. Sarma, S. Rayaprol, and E.-V. Sampathkumaran, Phys. Rev. B **71**, 073406 (2005).
[37] M. Senthilkumar and R. Vijayaraghavan, Sci. Technol. Adv. Mater. **10**, 015007 (2009).
[38] S. Hébert, D. Flahaut, C. Martin, S. Lemonnier, J. Noudem, C. Goupil, A. Maignan, and J. Hejtmanek, Prog. Solid State Chem. **35**, 457 (2007).
[39] T. Takami and H. Ikuta, Proceedings of the 24th International Conference on Thermoelectrics (ICT2005) (IEEE, Piscataway, 2005), pp. 492–495.
[40] A. Maignan, V. Caignaert, B. Raveau, D. Khomskii, and G. Sawatzky, Phys. Rev. Lett. **93**, 026401 (2004).
[41] H. Wu, M. W. Haverkort, Z. Hu, D. I. Khomskii, and L. H. Tjeng, Phys. Rev. Lett. **95**, 186401 (2005).
[42] A. Kosuga, K. Kurosaki, K. Yubuta, A. Charoenphakdee, S. Yamanaka, and R. Funahashi, Jpn. J. Appl. Phys. **48**, 010201 (2009).